Title

STRUCTURE AND MECHANICAL BEHAVIOR OF SPINODALLY DECOMPOSED Cu-Ni-Fe ALLOYS OF ASYMMETRICAL COMPOSITION.

Author

Livak, R.J.

Publication Date

1970-03-01

UCRL-19189

c.2

STRUCTURE AND MECHANICAL BEHAVIOR OF SPINODALLY DECOMPOSED Cu-Ni-Fe ALLOYS OF ASYMMETRICAL COMPOSITION

R. J. Livak
(M.S. Thesis)

March 1970

AEC Contract No. W-7405-eng-48

LAWRENCE RADIATION LABORATORY
UNIVERSITY of CALIFORNIA BERKELEY

UCRL-19189

25

DISCLAIMER

Contents

STRUCTURE AND MECHANICAL BEHAVIOR OF SPINODALLY DECOMPOSED Cu-Ni-Fe ALLOYS OF ASYMMETRICAL COMPOSITION

R. J. Livak

Inorganic Materials Research Division, Lawrence Radiation Laboratory, Department of Materials Science and Engineering, College of Engineering, University of California, Berkeley, California

ABSTRACT

Two Cu-Ni-Fe alloys of asymmetrical composition (i.e. with unequal volume fractions of the two low temperature phases) were heat treated to produce spinodal structures with various wavelengths or characteristic particle spacings. Transmission electron microscopy and diffraction were used to study the spinodally decomposed microstructures and to measure the wavelengths in the specimens. Tensile tests were performed to measure mechanical properties of the aged specimens, and the fracture characteristics were studied by scanning electron microscopy. The change in composition of the Ni-Fe rich phase with aging time was determined by measuring the Curie temperature. The experimental results for the transformation kinetics agree with Cahn's diffusion theory during the later stages of spinodal decomposition. While coherency is maintained, the yield stress is found to be directly proportional to the difference in cubic lattice parameters of the two precipitating phases and is independent of the wavelength and the volume fractions.

INTRODUCTION

The concept of the spinodal was formulated at the same time as nucleation theory, and both concepts were discussed in the same paper by Willard Gibbs[1] in 1877. On a phase diagram, the spinodal is given by the thermodynamic condition that the second derivative of the free energy with respect to composition is zero ($d^2f/dc^2 = 0$). Inside the spinodal where $d^2f/dc^2 < 0$ the unstable solid solution decomposes spontaneously into two phases because there is no activation barrier for nucleation as in a metastable solid solution. Thus, Gibbs referred to the spinodal as the limit of metastability. Spinodal decomposition is characterized by small composition fluctuations over large distances, whereas, a classical nucleation process is characterized by large composition variations over small distances. In solids, spinodal decomposition implies that the new phases form by a continuous process; and thus the new phases must have similar crystal structures as the original solid solution. The two phases are initially coherent and the crystal structure is continuous.

A diffusion theory describing the mechanism of spinodal decomposition has been developed by Hillert[2] and Cahn[3,4] based on changes in the solution free energy with composition fluctuations in the unstable solid solution. The solution to the derived diffusion equation can be mathematically expressed as the superposition of periodic composition waves in the solid solution with an exponential time dependence. Included in the diffusion equation are terms for the coherency strain energy and the concentration gradient energy. The microstructure predicted by this theory is a periodic distribution of small, coherent particles or

regions of the two phases throughout the entire volume. The large strengthening effect resulting from this homogeneous distribution of two phases has been treated theoretically by considering the effect of the internal stresses[5,6] and the periodic variation of the elastic shear modulus due to the composition fluctuations.[7] Also, a model for the work hardening of a spinodally decomposed alloy has been proposed based on the disregistry strain produced by the passage of dislocations through the coherent particles.[8] A recent review article by Cahn[9] explains the current state of knowledge and important features of this transformation.

In elastically anisotropic materials, spinodal decomposition occurs along elastically "soft" directions; and for Cu-Ni-Fe alloys such directions are the cube directions. The resulting periodic structure produces side bands in diffraction patterns, and this effect has been studied extensively by x-ray investigators. Daniel and Lipson were the first to observe the sideband effect in Cu-Ni-Fe alloys, and they derived a formula relating the sideband spacing to the structural periodicity.[10]

The microstructure of a spinodally decomposed alloy can be characterized by three parameters:

(1) Volume fraction of the two phases

(2) Wavelength

(3) Amplitude of the composition fluctuations

Butler[11] studied a Cu-Ni-Fe alloy of symmetrical compositon (i.e. at the center of the miscibility gap) and followed the changes in wavelength and amplitude as a function of aging time. He also related the changes in microstructure to the age-hardening response of the alloy. The objective of the present investigation was to determine experimentally the effect of volume fraction on the transformation kinetics and on the age-

hardening response of Cu-Ni-Fe alloys. Two alloys of asymmetrical composition, which were on the same tie-line as the alloy studied by Butler, were heat treated to produce a spinodal structure; and the changes in microstructure and wavelength with aging time were followed by transmission electron microscopy (TEM) and diffraction. The amplitudes of the composition fluctuations were determined by measuring the Curie temperature, which is a function of composition, of the ferromagnetic Ni-Fe rich phase. Also, the mechanical behavior of the spinodally decomposed and aged alloys was experimentally studied.

The ternary Cu-Ni-Fe equilibrium phase diagram is shown in fig. 1. The 625°C solubility limit and the tie-line are taken from the work of Köster and Dannöhl.[12] The pseudo-binary phase diagram used in this investigation is given in fig. 2. The solvus curve and the variation of Curie temperature with compositon for quenched alloys are also taken from the work of Köster and Dannöhl. Butler calculated the position of the chemical spinodal curve using the formula derived by Cook and Hilliard.[13] The effect of coherency strains was not included in calculating the position of this curve; but coherency strains are small in these Cu-Ni-Fe alloys as shown by lattice parameter determinations and electron microscopy.

Decomposition of the high temperature fcc γ phase gives a paramagnetic Cu rich phase and a ferromagnetic Ni-Fe rich phase which both have fcc structures. Because the two low temperature phases are initially coherent and have different specific volumes, there are coherency strains in this spinodal microstructure. Dahlgren[6] has calculated the yield stress of alloys with coherent lamellar microstructures, and his theory is based on the elastic strains requried to maintain coherency between the two

phases. The conclusions reached by Dahlgren in his calculations are that the yield stress of spinodally decomposed Cu-Ni-Fe alloys depends on the difference in cubic lattice parameters of the two phases and is independent of the wavelength and of the volume fractions of the precipitating phases between certain critical values. Dahlgren's results were partially confirmed by the experimental work of Butler;[11] however, the effect of volume fraction on the yield stress was not studied by Butler. The objective of this research was to continue the investigation of spinodally decomposed Cu-Ni-Fe alloys by studying two alloys of asymmemtrical compositions and correlating the mechanical behavior with the changes in microstructure during spinodal decomposition and particle coarsening.

EXPERIMENTAL PROCEDURE

The experimental alloys were prepared using 99.999% purity Cu, 99.85% purity Ni and 99.6% purity Fe. The compositons of the two alloys, in atomic percent, were:

alloy 1, 32.0 Cu-45.5 Ni-22.5 Fe;

alloy 2, 64 Cu-27 Ni-9 Fe.

To aid fabrication, 0.5% Mn was added to each melt to act as a deoxidizer. The charges were melted in a large induction furnace in an helium atmosphere and were chill cast into copper molds to reduce segregation. X-ray fluorescent analysis verified to within ±1% the compositions given above.

The ingots were inserted into stainless steel envelopes and placed inside an Inconel tube filled with cast iron chips and a small amount of activated charcoal to prevent oxidation. Then the ingots were homogenized at 1050°C for three days. Next the ingots were hot forged and rolled at 950°C to a thickness of 40 mils. Small pieces from each ingot were then annealed and further cold rolled to 8 mils thickness for TEM specimens.

After cutting and machining the various experimental specimens, they were encapsulated in evacuated quartz tubes, solution treated at 1050°C for two hours and then quenched in water. To ensure that the specimens had not spinodally decomposed before starting the aging treatments, the specimens were further heat treated at 1050°C for 15 minutes in purified argon and then drop quenched into stirred ice brine. The quenching rate was estimated to be about 5000°C/min. After this heat treatment, alloy 1 specimens had an average grain diameter of 0.07 mm and for alloy 2 specimens 0.12 mm diameter. Then groups of specimens were aged at 625°C for 1 minute, 0.1, 1, 10, 100 and 1000 hours. For aging times less than one hour, a salt

bath was used.

An Instron testing machine was used to measure the yield stress and ductility of flat tensile specimens which were 40 mils thick with a 1" gage length, a 1/8" gage width and 1/4" diameter pin holes. Three tensile specimens for each aging time were tested at room temperature, and all specimens were pulled at a constant strain rate of 0.02 cm/min. The yield stress was measured at 0.2% strain offset, and the total elongation to fracture was determined by the change in spacing of two indentations made on the gage length. The work hardening rate (i.e. the slope of the stress-strain curve) was calculated at 2% strain for all specimens tested. A scanning electron microscope was used in examining the fracture surfaces to determine the mode of fracture.

To determine the compositon of the Ni-Fe rich phase, the Curie temperatures of the aged specimens were measured using apparatus developed at LRL Livermore for the study of high temperature magnetic phase changes.[14] This apparatus is essentially a transformer in which the specimen is the core between the primary and secondary coils. Because the apparatus is made of boron nitride, quartz tubing and platinum wire, it can be heated inside a furnace to temperatures not exceeding 850°C. An X-Y recorder was used to measure the change in induced voltage of the secondary coil as a function of temperature. Two heating and cooling cycles were run for each specimen, and the average value of the measured temperatures was taken as the Curie temperature. The specimens used for this measurement were 1" x 1/4" x 40 mils.

The heat treated coupons used to prepare thin foils for transmission electron microscopy measured 1" x 1/2" x 8 mils. The coupons were first

thinned chemically with the following polish.

20 ml acetic acid

10 ml nitric acid

4 ml hydrochloric acid

This chemical polish, diluted with an equal amount of water, was also used to remove a black oxide which sometimes formed on the specimens during electropolishing. Thin foils were obtained using the following electrolyte and polishing conditions.

50 gm CrO_3

260 ml acetic acid

8 - 10 ml H_2O

Temperature: 10°C

Voltage: 14 - 19 V dc

Slow stirring of the electrolyte

The best polishing voltage varied with the heat treatment of the specimen.

The wavelengths (λ) or particle spacings of heat treated specimens were measured directly from enlarged prints of micrographs. All micrographs were taken in the <110> orientation with a strong 200 reflection operating. At least one hundred measurements, taken from five different areas, were made to determine the average wavelength for each aging time. Because a 15% magnification error can occur when using a double tilt specimen stage, a carbon replica of a ruled grating was used to calibrate the magnification for different objective lens currents at fixed settings of the intermediate and projector lenses. For specimens with $\lambda < 150$Å, the sideband spacings on 400 reflections were also used to calculate λ from the formula[10]

$$\lambda = \frac{h \tan \theta}{(h^2 + k^2 + \ell^2)\delta\theta} \, a_o$$

where θ is the Bragg angle for the hkℓ reflection in a crystal of lattice parameter a_o and $\delta\theta$ is the angular spacing between sideband and main reflection. For the 400 reflection in these Cu Ni-Fe alloys this equation reduces to

$$\lambda = 0.89 \frac{r}{\Delta r}$$

where r and Δr are the distances from 000 and the sideband to the 400 reflection. A Joyce-Loebl double beam recording microdensitometer was used to measure these distances directly from the diffraction patterns along a trace parallel to the [100] direction on the pattern.

EXPERIMENTAL RESULTS

The experimental results for the two alloys studied are summarized in tables 1 and 2 and in the graphs shown in figures 3 and 4. For comparison, Butler's results[11] for the Cu-Ni-Fe alloy of symmetrical composition aged at 625°C are given in figure 5. The compositions of the Ni-Fe rich phase were determined from the Curie temperature measurements using the information given in Butler's report (see figure 2). Distinct sideband peaks were not observed on the microdensitometer traces, but rather a general flattening of the main diffracted peak was observed to occur over some finite distance on the diffraction pattern (see fig. 6). Thus, the values of λ calculated from the sideband spacings represent some average wavelength in the microstructure. The wavelength values determined from the sidebands give a more accurate measurement of the actual wavelengths than the micrographs because a diffraction pattern represents a larger statistical sampling of the specimen than the one hundred measurements taken from micrographs. Also, there is no possible magnification error in the sideband measurements.

The changes in microstructure with aging time for alloy 2 are shown in the transmission electron micrographs of figures 7a-e and 8a-b. Alloy 1 showed a similar development of microstructure. For $\lambda < 150$Å, the microstructure consists of wavy, irregular plates or rods lying primarily along (100) planes. Even in the specimen aged ten hours, it is difficult to discern a distinct interface between the two decomposing regions. The last two micrographs of specimens aged 100 and 1000 hours show that definite, coherent interfaces parallel to (100) planes have developed between the Cu rich and Cu poor phases. The fringes observed on the micrograph in figure 8a

are thickness fringes resulting from the preferential polishing of the Cu rich phase. Micrographs of alloy 1 and the symmetrical alloy are also given in figure 8 for comparison of the three microstructures and to show the interconnectivity of the two phases.

Cadoret and Delavignette[15] studied the contrast in the electron microscope of spinodally decomposed Cu-Ni-Fe alloys and concluded that the contrast results from atomic displacements in the direction of the composition fluctuations or waves. They experimentally verified this contrast mechanism by showing that the contrast reversed with a change in the sign of the diffraction vector, $\bar{g}$. As indicated by the Curie temperature measurements, the as quenched specimens had partially decomposed. But because the amplitude of the composition fluctuations was small, the atomic displacement between the Cu rich and Cu poor regions was small. Thus the contrast in the as quenched specimen was weak (see fig. 7a). For specimens aged up to one hour, the observed contrast became stronger with increased aging time as the composition amplitude increased (see figures 7b-d).

A comparison of the measured Curie temperatures and the wavelengths show that the wavelength did not grow significantly until the equilibrium tie-line compositions were reached (cf. tables 1 and 2 with fig. 2). Then particle coarsening occurred as shown in figures 7e and 8a-b, and the two phases remained coherent after aging for 1000 hours at 625°C. Optical metallography revealed some discernible grain boundary precipitation after aging for 10 hours, a few discrete grain boundary precipitates after 100 hours and some continuous grain boundary precipitation after 1000 hours (see fig. 9).

The yield stress of the spinodally decomposed alloys increased threefold with longer aging times until the equilibrium tie-line compositons were reached; and there was a corresponding 75% decrease in the total strain to fracture. For alloy 1, the yield stress decreased slightly for specimens aged longer than 10 hours; whereas alloy 2 showed no change in yield stress for specimens aged 10 hours up to 1000 hours. The work hardening rate ($d\sigma/de$) measured at 2% strain increased with aging time for both alloys tested. While alloy 1 showed a twofold increase in the work hardening rate, alloy 2 had only a 25% increase after aging for 1000 hours. Fractography revealed that the as quenched specimen and the specimen aged one minute fractured in a completely ductile manner. With increased aging time, the fracture mode became intergranular with some small regions of ductile failure (see fig. 10).

DISCUSSION

The rates of spinodal decomposition for the symmetrical and asymmetrical Cu-Ni-Fe alloys were found to be significantly different; and a comparison of the present results with Butler's results for the symmetrical alloy on the same tie-line shows this difference (see figures 3, 4, and 5). Butler found that the as quenched symmetrical alloy showed no evidence of decomposition and that the equilibrium compositions were reached after aging for one hour at 625°C. But for the asymmetrical alloys, the as quenched specimens had partially decomposed and the equilibrium compositions were reached after aging for ten hours at 625°C.

This rate difference can be understood physically by considering the free energy curve and the driving force for spinodal decomposition. The reaction rate is proportional to the magnitude of the driving force which is the second derivative of free energy with respect to composition (d^2f/dc^2). Because the driving force is greater for the symmetrical alloy than for the asymmetrical alloys, spinodal decomposition occurs more rapidly in the symmetrical alloy. The difference in the as quenched structures was probably due to a difference in the quenching rates.

Once the asymmetrical alloys reached the equilibrium tie-line compositions, particle coarsening occurred (figures 3 and 4). A log-log plot of wavelength vs. aging time gave a time dependence exponent of ~0.37. That is, the observed rate law was $\lambda \propto kt^{0.37}$. However, this value is only approximate because of the small number of data points plotted and the scatter of the data points about the straight line with slope of 0.37. For the symmetrical alloy, Butler[11] found that particle coarsening could be described by the rate law $\lambda \propto kt^{1/3}$, which is consistent with

the theories of diffusion controlled coarsening where large spherical particles grow at the expense of small ones.

A comparison of the Curie temperature data (tables 1 and 2) with the pseudo-binary diagram (fig. 2) indicates that the as quenched specimens of both alloys had partially decomposed to the spinodal composition, as given by the tie-line, that was nearest to the original alloy composition. Note that for both as quenched alloys, the measured compositions of the Ni-Fe rich phase were $\pm$ 8% Cu from the original compositions. Thus, during the quench, the fundamental composition wave developed. The fundamental can be described by a sine wave form and is symmetrical about the original composition. As the fundamental grows in amplitude upon aging, the non-linear terms in the solution of the diffusion equation for spinodal decomposition become important and they produce harmonic distortions of the fundamental composition waves.

As discussed by Cahn,[16] the amplitudes of these harmonic distortions are proportional to the square or higher power of the fundamental amplitude; and when this amplitude is initially small, these distortions are not important. The even harmonics, which have non-zero amplitudes only in asymmetrical alloys, distort the fundamental sine wave to conform to the lever rule by increasing the amplitude of the minor phase while decreasing its spatial extent and vice versa for the major phase (see fig. 11). This effect of the even harmonics is clearly shown in the Curie temperature data for alloy 2 aged from one minute up to ten hours. The odd harmonics convert the fundamental sine wave into a square wave, i.e. a composition profile more characteristic of a two phase structure, by

flattening the peaks of the fundamental and sharpening the gradient between the extremes in composition. As the gradient at the interface increases, the contrast between adjacent particles also increases and the interface becomes more distinct. This effect is qualitatively seen in the series of electron micrographs of the aged specimens (fig. 7a-e).

This simple explanation of spinodal decompositon describes the average or overall decompositon process occurring throughout the specimen. But within a localized region the actual decomposition process is more complicated than suggested above because there are several wavelengths present and the effects of the harmonics on the fundamental wave cannot be so precisely described. The microdensitometer trace of a 400 diffraction spot given in figure 6 shows three distinct sideband peaks to the right of the main peak. Thus, the crystal contained a spectrum of wavelengths centered about the dominant wavelength that received maximum amplification. Also, during the initial stages of spinodal decompositon when the wave amplitudes are small, the elastic strain energy term is not very large for Cu-Ni-Fe alloys. Consequently, the crystal can be considered elastically isotropic during the early stages and the composition waves may not necessarily be along the cube directions.

The wavy appearance of the particles during the first ten hours of aging can be understood qualitatively by considering the changes in microstructure during spinodal decomposition of Cu-Ni-Fe alloys. Khachaturyan[17] has done an elastic energy analysis of a homogeneously decomposing solid solution and has shown that the distribution and shape of particles is determined by the minimum elastic energy associated with the difference in specific volumes of the precipitating phases. This elastic energy mechanism differs from Cahn's theory which is only valid

when the composition wavelength is commensurate with the correlation length (i.e. the measure of non-locality of free energy). Since the correlation length is the same order of magnitude as the thickness of the transitional boundary layer, Cahn's theory is only valid during the early stages of spinodal decomposition.

In a face centered cubic solid solution that decomposes along the cube axes, Khachaturyan has described the following steps in the development of the particle morphology, starting with the distribution of the highest energy and progressing to that of lowest energy.

1) Three-dimensional distribution described as a primitive cubic lattice the sites of which are cuboidal inclusions of the equilibrium phases and of partially decomposed matrix.
2) Two-dimensional distribution described as a planar square lattice formed by rod-shaped particles.
3) One-dimensional distribution of parallel lamellar particles that are regularly spaced.

Initially during the decomposition process, composition waves form in all three dimensions along the cube axes as noted by Cahn.[3] But this particle morphology transforms to the energetically favored two-dimensional distribution and then finally to the one-dimensional distribution. The total free energies of the multi-dimensional distributions are greater than that of the one-dimensional distribution because of differences in elastic energy and also in chemical free energy since the one-dimensional distribution contains only the equilibrium phases but the multi-dimensional distributions also contain some partially decomposed matrix.

For the asymmetrical alloys studied, the equilibrium compositions

were reached after ten hours of aging (cf. tables 1 and 2 with fig. 2). Thus, in specimens aged less than ten hours, partially decomposed matrix was still present and the microstructure consisted of multi-dimensional distribution of particles. Because the particle morphology was transforming to the one-dimensional distribution, no distinct (100) habit planes developed until the specimens had been aged 100 hours. Consequently, the microstructure had a wavy appearance as observed in the electron micrographs (see fig. 7a-e).

The asymmetrical alloys have age-hardening responses similar to the symmetrical alloy, i.e. the yield stress increased rapidly with aging time and then became constant for aging times greater than ten hours. However, there is one significant difference between the two cases. For the asymmetrical alloys, the wavelength initially remained constant while the yield stress doubled. But for the symmetrical alloy, the wavelength grew initally as the yield stress increased (cf. figures 3, 4, and 5). Then as the wavelength increased for aging times greater than ten hours, the yield stress remained constant. But the variation of yield stress for the asymmetrical alloys followed approximately the change in Curie temperature (i.e. compositon) of the Ni-Fe rich phase (see fig. 12). Assuming that the lattice parameter is proportional to the composition, the yield stress of the spinodally decomposed, asymmetrical Cu-Ni-Fe alloys is directly proportional to the difference in cubic lattice parameters of the two coherent phases and is independent of the wavelength. Also, the symmetrical and asymmetrical alloys aged at 625°C attained about the same maximum yield stress (35-39 kg/mm^2). Therefore, the yield stress is not a function of the volume fractions of the precipitating phases for the case when the volume fraction of the minor phase is not less than one-fourth.

The yield stress dependence on the various microstructural parameters observed in this study agrees completely with the conclusions reached by Dahlgren[6] for his theoretical calculation of the yield stress of alloys with coherent lamellar microstructures. Dahlgren's theory was based on the internal coherency strains resulting from the difference in lattice parameters of the two precipitating phases. He calculated the internal stress field for the lamellar microstructure and then resolved these stresses along the slip plane in order to determine the applied stress required for the initial passage of dislocations through the microstructure. Note that the physical basis for this calculation was the same one as used by Mott and Nabarro[18] to derive the following expression for the average internal stress due to spherical, coherent precipitates.

$$\sigma_i \sim 2G\varepsilon f$$

In this expression, G is the average shear modulus, ε is the misfit parameter between solute and solvent atoms and f is the volume fraction of the precipitating phase.

As a result of his calculations, Dahlgren concluded that:

1) The yield stress is independent of the wavelength, λ.
2) The yield stress is nearly independent of the volume fractions f_1 and f_2 if the elastic constants do not differ appreciably in the two phases and if for an isotropic material the condition $1/3 \leq f_1 \leq 2/3$ is satisfied.
3) The yield stress is directly proportional to the difference in cubic lattice parameters of the precipitating phases when the same conditions as in (2) apply.

Because Cu-Ni-Fe alloys are anisotropic and the elastic constants of

the precipitating phases differ by a small amount, the limits given above for the volume fraction are only approximate. In this present study of asymmetrical alloys, it was found experimentally that the limits on the volume fraction are $1/4 \leq f_1 \leq 3/4$ for the above conclusions to be valid.

As long as the minor phase remains interconnected, it is physically reasonable to expect the yield stress to be independent of the volume fraction. Because given the interconnectivity of the minor phase, the dislocations must pass through the coherent interfaces and cannot cross slip around the particles. Cahn[19] did a computer simulation for the spinodally decomposed microstructure of an isotropic material and found that with 0.24 volume fraction the minor phase remained interconnected. The transition to isolated particles was found to occur in the volume fraction range of 0.15 ± 0.03. The electron micrographs in figures 7 and 8 show that the minor phase in the Cu-Ni-Fe alloys was interconnected at a volume fraction of 0.25.

The work hardening rate ($d\sigma/de$) of both alloys studied increased with aging time (see tables 1 and 2); and alloy 1 showed a larger increase than alloy 2. Carpenter[8] has proposed a model for the work hardening rate of spinodally decomposed alloys based on the lattice disregistry shear strain resulting from the passage of dislocations through the coherent particles. The derived total flow stress for the alloy in the plastic region is

$$\sigma_t = \sigma_y + \frac{\sqrt{2}\Delta a}{a_o} G \sin \frac{2\pi nb}{\lambda}$$

where σ_y is the yield stress, Δa is the maximum difference in lattice

parameters of the decomposing regions, a_o is the lattice parameter of the quenched solid solution, G is the shear modulus, n is the number of dislocations which have passed through the matrix, b is the Burgers vector and λ is the wavelength.

Carpenter noted that for fixed plastic strain (i.e. n constant) an increase in λ will cause a decrease, rather than an increase, in the work hardening rate. But the experimental results for alloy 1 show a significant difference between the work hardening rates for the specimen aged 10 hours and the one aged 1000 hours where λ increased by a factor of eight and Δa for the two specimens remained about constant. This discrepancy between the derived equation and experimental results indicates that Carpenter's model may only be valid for small plastic strains (i.e. less than 2%) before the coherent microstructure has been greatly distorted by the passage of dislocations through it. The observed differences in the work hardening rates of alloy 1 and alloy 2 suggest that there may be other factors not considered in Carpenter's model which influence the work hardening rate of spinodally decomposed alloys. For example, the work hardening rate may depend on the relative volume fractions of the precipitating phases and on the difference in shear moduli of the two decomposing regions. Also, the functional dependence of $d\sigma/de$ on λ is probably different than that derived by Carpenter.

The fractography results showed that the as quenched specimen and the specimen aged for one minute failed in a transgranular ductile manner. However, the specimens aged six minutes and longer failed intergranularly with some areas of ductile fracture. Using optical metallography, no grain boundary precipitates were detected in specimens

aged for times less than 10 hours. This change in fracture mode is probably explained by the increase in yield stress and work hardening rate with aging time. The grain boundaries have some given fracture strength that is not strongly dependent on the microstructure of the matrix. In the as quenched specimen and the one aged for one minute, the fracture stress of the matrix was less than the fracture stress of the grain boundaries. But in the specimens aged six minutes and longer, just the reverse situation occurred and the fracture stress of the grain boundaries was reached before the matrix failed. However, this explanation is tentative as there are other microstructural factors (e.g. grain boundary segregation) that may be causing the intergranular fracture of the aged specimens.

SUMMARY

In this experimental study of spinodally decomposed Cu-Ni-Fe alloys of asymmetrical compositions, the following results were obtained.

1) The as quenched specimens contained the fundamental composition waves which formed during the quench. With aging, this initial sine wave, or first harmonic, was distorted by higher order harmonics which resulted in a square wave profile for the composition fluctuations.
2) The quenched-in fundamental wavelength did not grow until the equilibrium tie-line compositions were reached. Note that this result differed from that for the symmetrical alloy in which the wavelength began growing immediately upon aging before the equilibrium tie-line compositions were reached.
3) The reaction rate for spinodal decomposition of the asymmetrical alloys was one order of magnitude slower than for the symmetrical alloy.
4) For this coherent microstructure in the spinodally decomposed alloys of asymmetrical composition, the yield stress is directly proportional to the difference in cubic lattice parameters of the two precipitating phases and is independent of the wavelength and the relative volume fractions within the limits $1/4 \leq f_1 \leq 3/4$.

ACKNOWLEDGEMENTS

The author would like to express his appreciation to Professor Gareth Thomas for his advice and encouragement during this study. He is also grateful to Dr. E. P. Butler and Dr. P. Okamoto for many helpful discussions and suggestions during the course of the work and wishes to thank Dr. A. Goldberg of Lawrence Radiation Laboratory, Livermore, for the loan of the Curie temperature apparatus. The research was supported by the U.S. Atomic Energy Commission through the Inorganic Materials Research Division of the Lawrence Radiation Laboratory, Berkeley, California.

TABLE I

EXPERIMENTAL DATA FOR

ALLOY 1: 32.0 Cu - 45.5 Ni - 22.5 Fe

AGING TIME	λ IN Å (MICROGRAPHS)	λ IN Å (SIDEBANDS)	CURIE TEMPERATURE	% Cu IN Ni-Fe PHASE	YIELD STRESS (kg/mm^2)	TOTAL % ELONGATION	$d\sigma/de$ (kg/mm^2)
AS QUENCHED	65 ± 8	--	420°C	24.3	13.2 ± 1.8	42.0 ± 0.2	104
1 MIN.	56 ± 7	66	440°C	21.8	15.6 ± 0.3	32.6 ± 2.4	122
0.1 HR.	73 ± 7	67	450°C	20.3	18.9 ± 0.7	17.8 ± 2.9	128
1 HR.	65 ± 7	62	470°C	17.2	27.0 ± 1.1	14.0 ± 4.5	144
10 HRS.	106 ± 7	138	505°C	11.5	36.0 ± 1.0	11.1 ± 4.0	122
100 HRS.	471 ± 17	--	496°C	13.2	33.5 ± 0.6	9.7 ± 0.4	178
1000 HRS.	827 ± 51	--	505°C	11.5	33.4 ± 0.9	9.1 ± 1.9	218

TABLE II

EXPERIMENTAL DATA FOR

ALLOY 2: 64 Cu - 27 Ni - 9 Fe

AGING TIME	λ IN Å (MICROGRAPHS)	λ IN Å (SIDEBANDS)	CURIE TEMPERATURE	% Cu IN Ni-Fe PHASE	YIELD STRESS (kg/mm^2)	TOTAL % ELONGATION	$d\sigma/de$ (kg/mm^2)
AS QUENCHED	71 ± 10	--	148°C	56.2	13.3 ± 0.7	30.6 ± 1.8	148
1 MIN.	74 ± 5	68	216°C	51.8	17.9 ± 0.1	19.3 ± 2.7	164
0.1 HR.	80 ± 9	78	319°C	38.5	23.8 ± 0.4	14.2 ± 1.1	164
1 HR.	62 ± 2	78	338°C	36.0	34.5 ± 0.3	8.8 ± 0.4	132
10 HRS.	124 ± 14	140	419°C	24.3	37.8 ± 0.8	7.5 ± 1.0	154
100 HRS.	577 ± 36	--	489°C	13.9	39.0 ± 1.2	7.1 ± 1.9	188
1000 HRS.	897 ± 44	--	495°C	13.2	38.6 ± 0.6	10.8 ± 1.2	188

REFERENCES

1. The Scientific Papers of J. Willard Gibbs, p. 105, Dover, 1961.
2. M. Hillert, Acta Met. 9, 525 (1961).
3. J. W. Cahn, Acta Met. 9, 795 (1961).
4. J. W. Cahn, Acta Met. 10, 179 (1962).
5. J. W. Cahn, Acta Met. 11, 1275 (1963).
6. S. D. Dahlgren, Ph. D. Thesis, University of California, Berkeley, UCRL Report # 16846 (1966).
7. D. N. Ghista and W. D. Nix, Materials Science Eng. 3, 293 (1969).
8. R. W. Carpenter, Ph. D. Thesis, University of California, Berkeley, UCRL Report# 16609 (1966).
9. J. W. Cahn, Trans. TMS-AIME, 242, 166 (1968).
10. V. Daniel and H. Lipson, Proc. Roy. Soc. 182, 378 (1943).
11. E. P. Butler, University of California, Berkeley, UCRL Report # 18840 (1969).
12. W. Köster and W. Dannöhl, Z. Metallk, 27, 220 (1935).
13. H. E. Cook and J. E. Hilliard, Trans. TMS-AIME, 233, 142 (1965).
14. A. Goldberg, W. U. Dent and J. H. Miller, J. Sci. Instrum. 44, 200 (1967).
15. R. Cadoret and P. Delavignette, Phys. Stat. Sol. 32, 853 (1969).
16. J. W. Cahn, Acta Met. 14, 1685 (1966).
17. A. G. Khachaturyan, Phys. Stat. Sol. 35, 119 (1969).
18. N. J. Mott and J. R. N. Nabarro, Proc. Phys. Soc. 52, 86 (1940).
19. J. W. Cahn, J. Chem. Phys. 42, 93 (1965).

FIGURE CAPTIONS UCRL-19189

Fig. 1. Ternary equilibrium diagram for the Cu-Ni-Fe system showing the tie-lines with the 625°C solvus line[12] and the compositions of alloys 1 and 2. Alloy A is the symmetrical alloy studied by Butler.[11]

Fig. 2. The pseudo binary section of the Cu-Ni-Fe system used in this investigation. X and Y are the expected equilibrium tie-line compositions of the decomposed phases when the alloys are aged at 625°C.[12] The chemical spinodal was calculated by Butler[11] using T_c ~ 825°C and C_c ~ 0.50 from ref. (13). The Curie temperatures of the quenched alloys were taken from ref. (12) except for the open circle which was measured by Butler for alloy A.

Fig. 3. Summary of the changes that occur in yield stress, Curie temperature and wavelength for alloy 1 aged at 625°C.

Fig. 4. Summary of the changes that occur in yield stress, Curie temperature and wavelength for alloy 2 aged at 625°C.

Fig. 5. Summary of the changes that occur in yield stress, Curie temperature and wavelength for alloy A aged at 625°C taken from ref. (11).

Fig. 6. Electron diffraction pattern of alloy 2 aged 1 hour at 625°C with microdensitometer trace showing the sidebands on the (400) reflection along the [100] direction. Note the three sideband peaks on the right which correspond to three wavelengths in the crystal.

Fig. 7. Transmission electron micrographs of alloy 2 (a) as quenched showing very faint contrast of the decomposing regions and aged

at 625°C for (b) 1 min. $\lambda \sim 75$Å, (c) 0.1 hr. $\lambda \sim 75$Å, (d) 1 hr. $\lambda \sim 75$Å, and (e) 10 hrs. $\lambda \sim 135$Å. Diffracting conditions are the same in all micrographs with $\bar{g} = (200)$ operating from left to right with foil orientation <110> as shown in the diffraction pattern (f).

Fig. 8. Electron micrographs of alloy 2 aged at 625°C for (a) 100 hrs. $\lambda \sim 575$Å and (b) 1000 hrs. $\lambda \sim 900$Å. Micrographs of alloy A taken from ref. (11): (c) aged at 700°C for 16 hrs. $\lambda \sim 500$Å, (d) aged at 775°C for 16 hrs. $\lambda \sim 975$Å. Micrographs of alloy 1 aged at 625°C for (e) 100 hrs. $\lambda \sim 470$Å and (f) 1000 hrs. $\lambda \sim 825$Å. The copper rich phase was preferentially electropolished, and in some foils this phase was completely removed as shown in (f). Note that no preferential precipitation occurred along the boundary shown in (f). These micrographs of the three alloys show that the two phases remained interconnected.

Fig. 9. Optical micrographs of alloy 2 aged at 625°C for (a) 10 hrs. and (b) 1000 hrs. showing that grain boundary precipitation occurs after aging for 10 hrs. and forms a grain boundary network after 1000 hrs.

Fig. 10. Scanning electron fractographs of alloy 2 (a) as quenched and aged at 625°C for (b) 1 min., (c) 0.1 hr. and (d) 1 hr. showing the abrupt change from transgranular, ductile failure to intergranular failure after aging for 0.1 hr.

Fig. 11. Effect of lever rule harmonics on the fundamental composition wave (from ref. 16):

(a) 1. The fundamental <100>.

2. The second harmonic <200>.

3. The harmonic distortion produced by adding the <200> in phase with the fundamental leads to a lever rule correction.

(b) Final shape of composition wave for asymmetrical alloy.

Fig. 12. Plot of yield stress vs. change in % Cu of the Ni-Fe rich phase as determined by the Curie temperature for alloys 1 and 2.

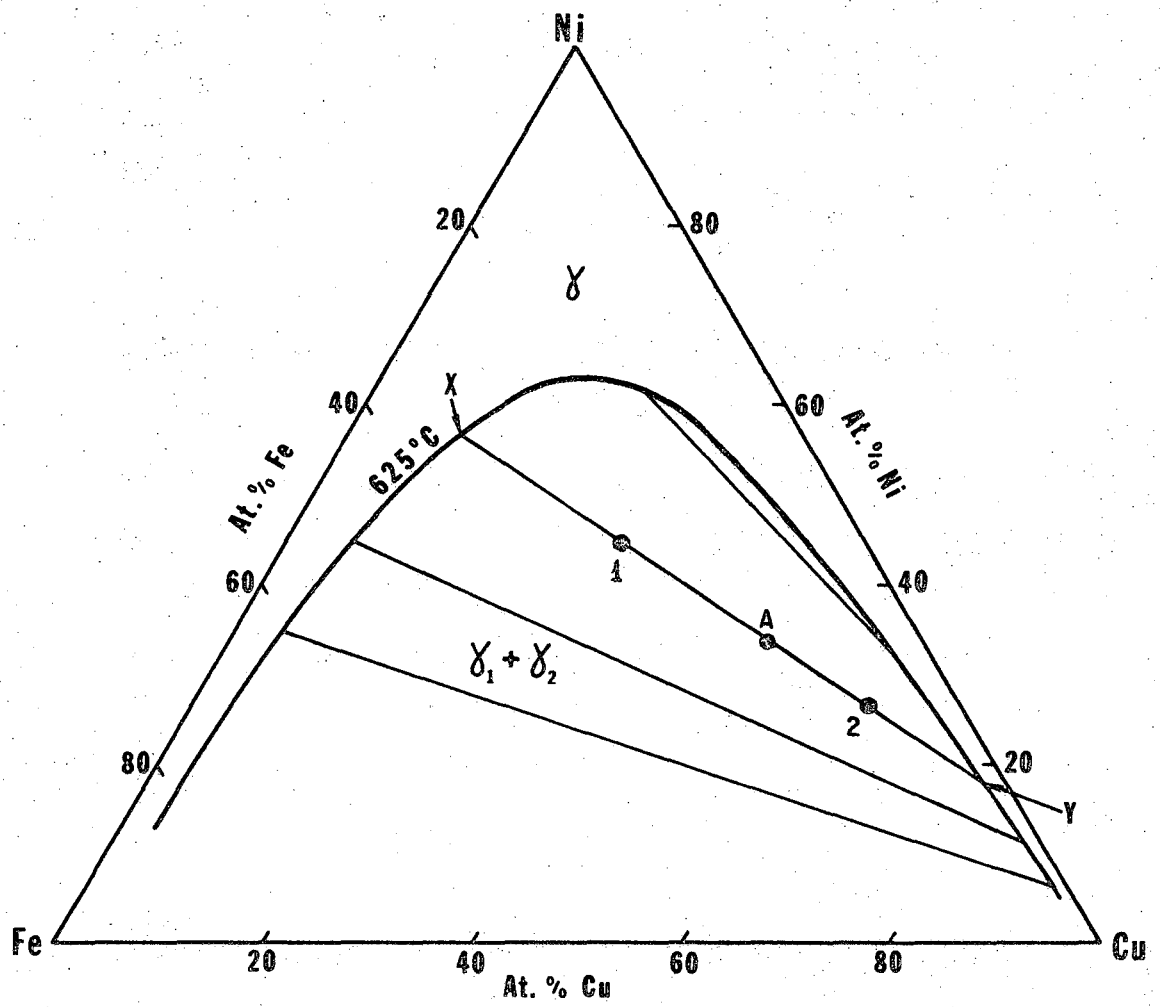

XBL 693-289

FIG. 1

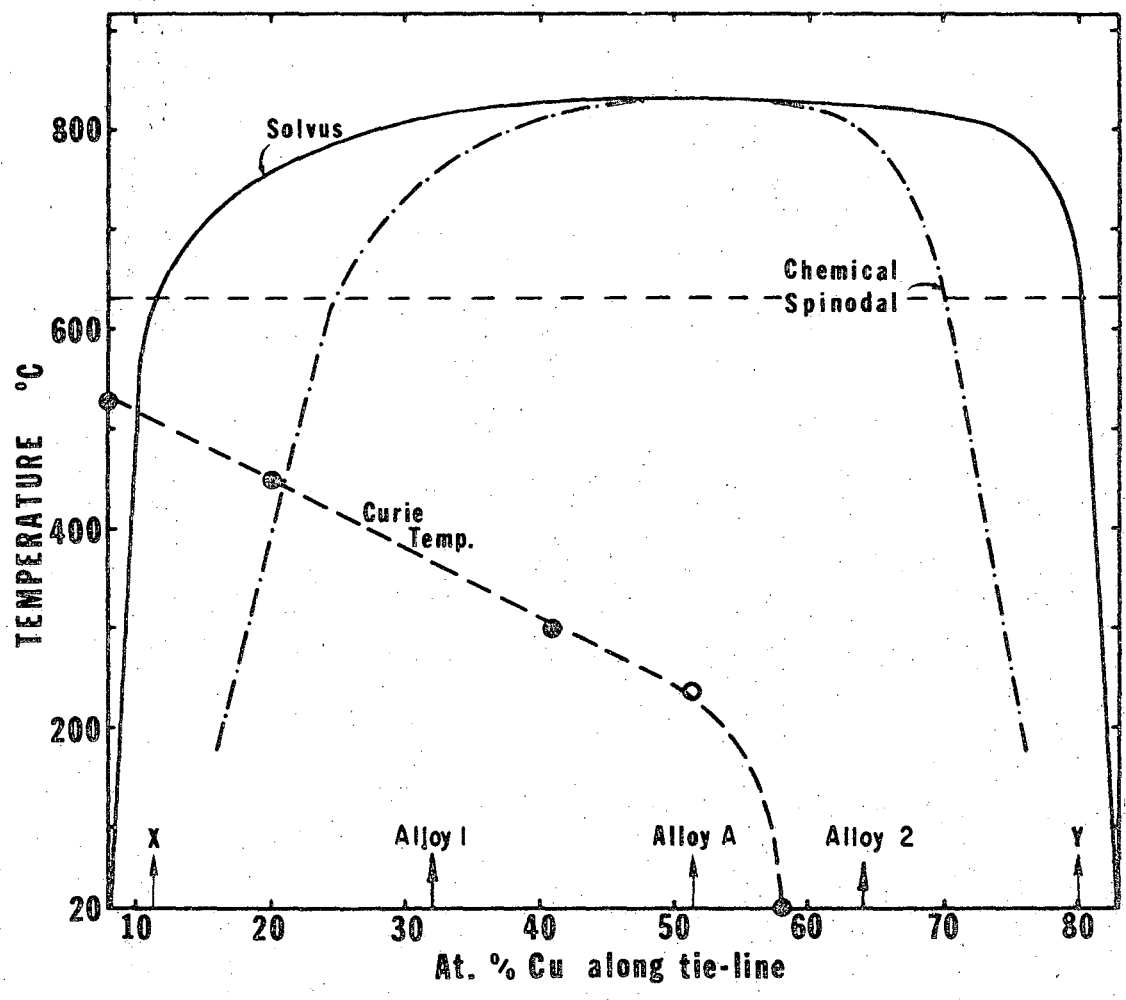

XBL 693-293

FIG. 2

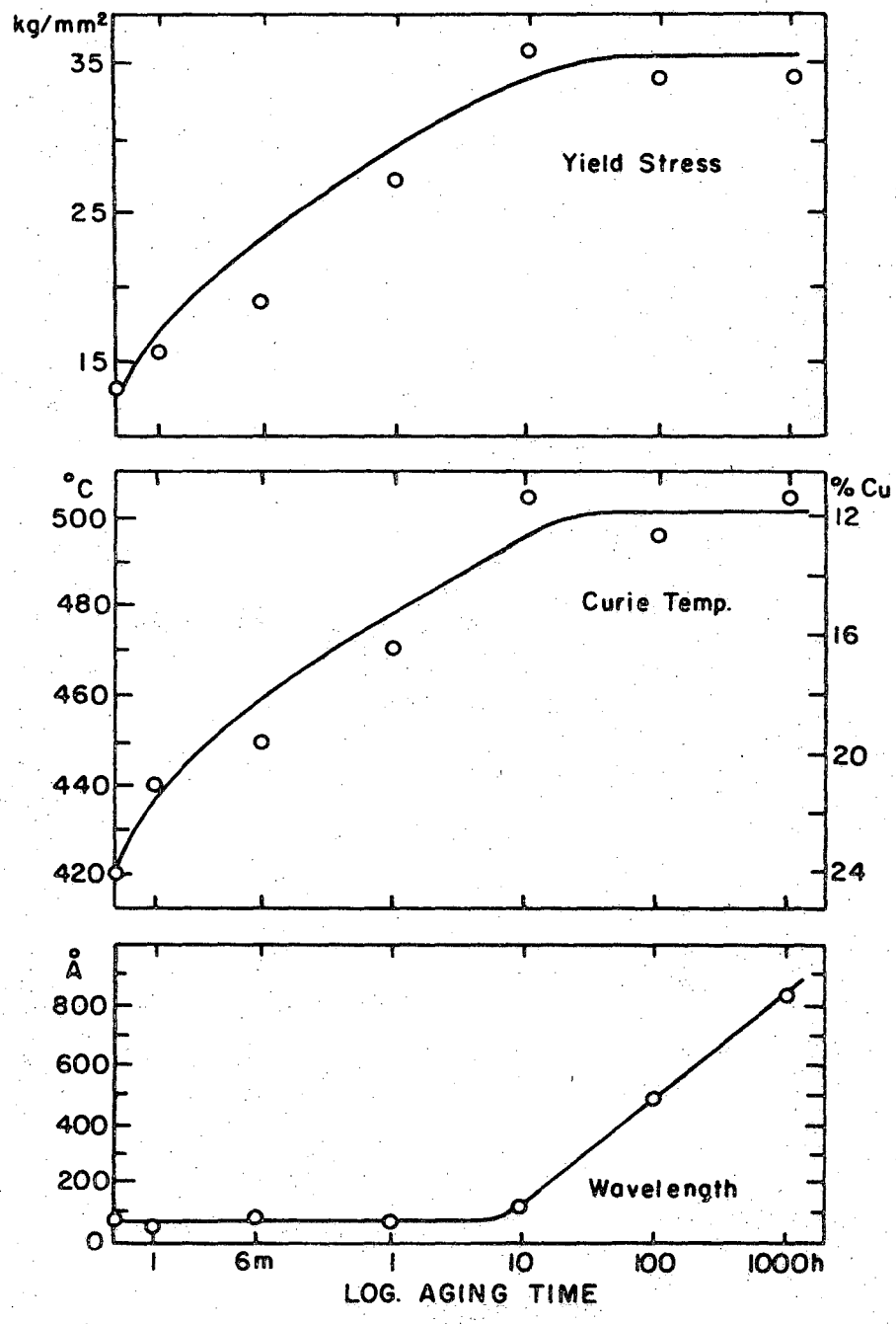

XBL 702-447

FIG. 3

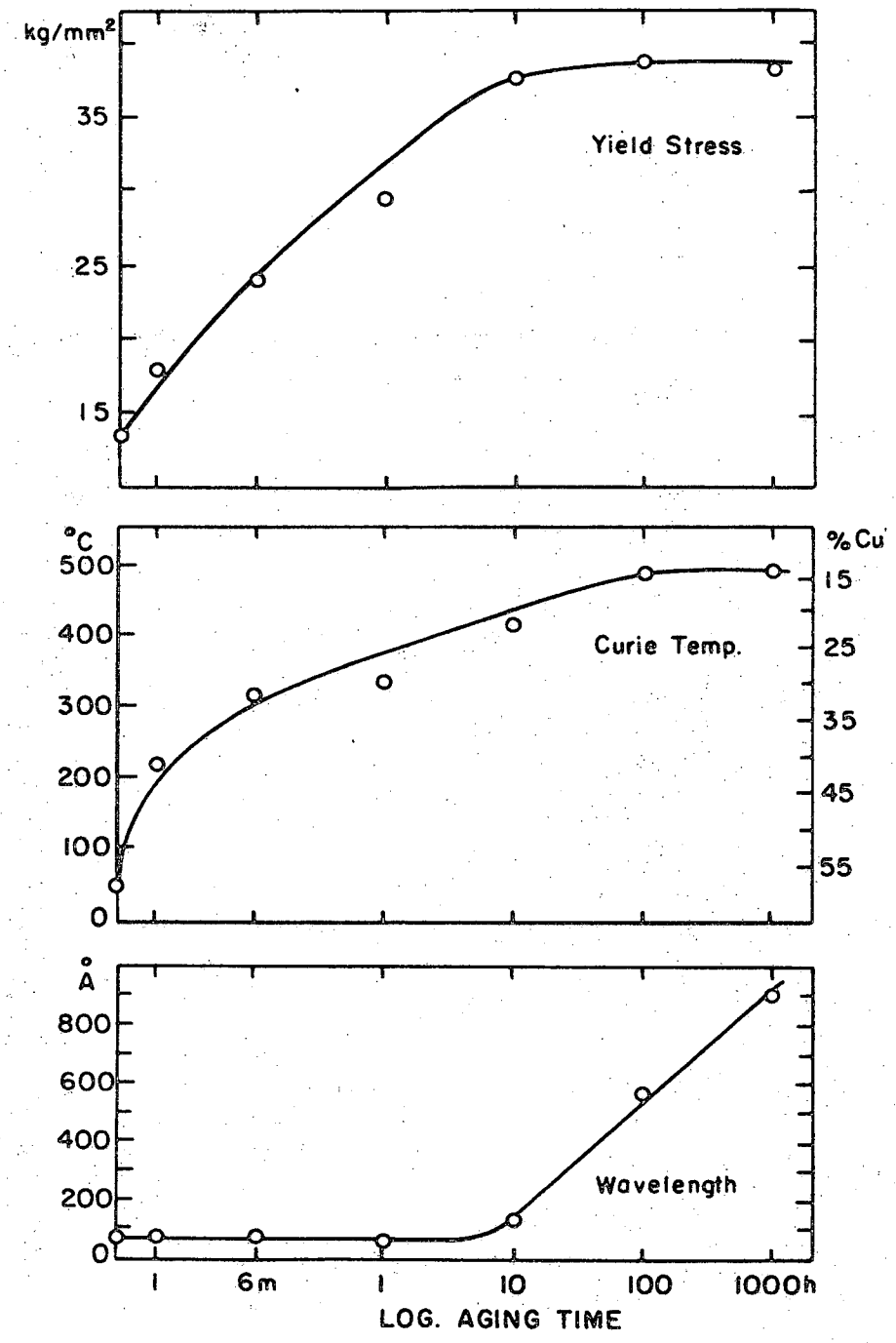

XBL 702-448

FIG. 4

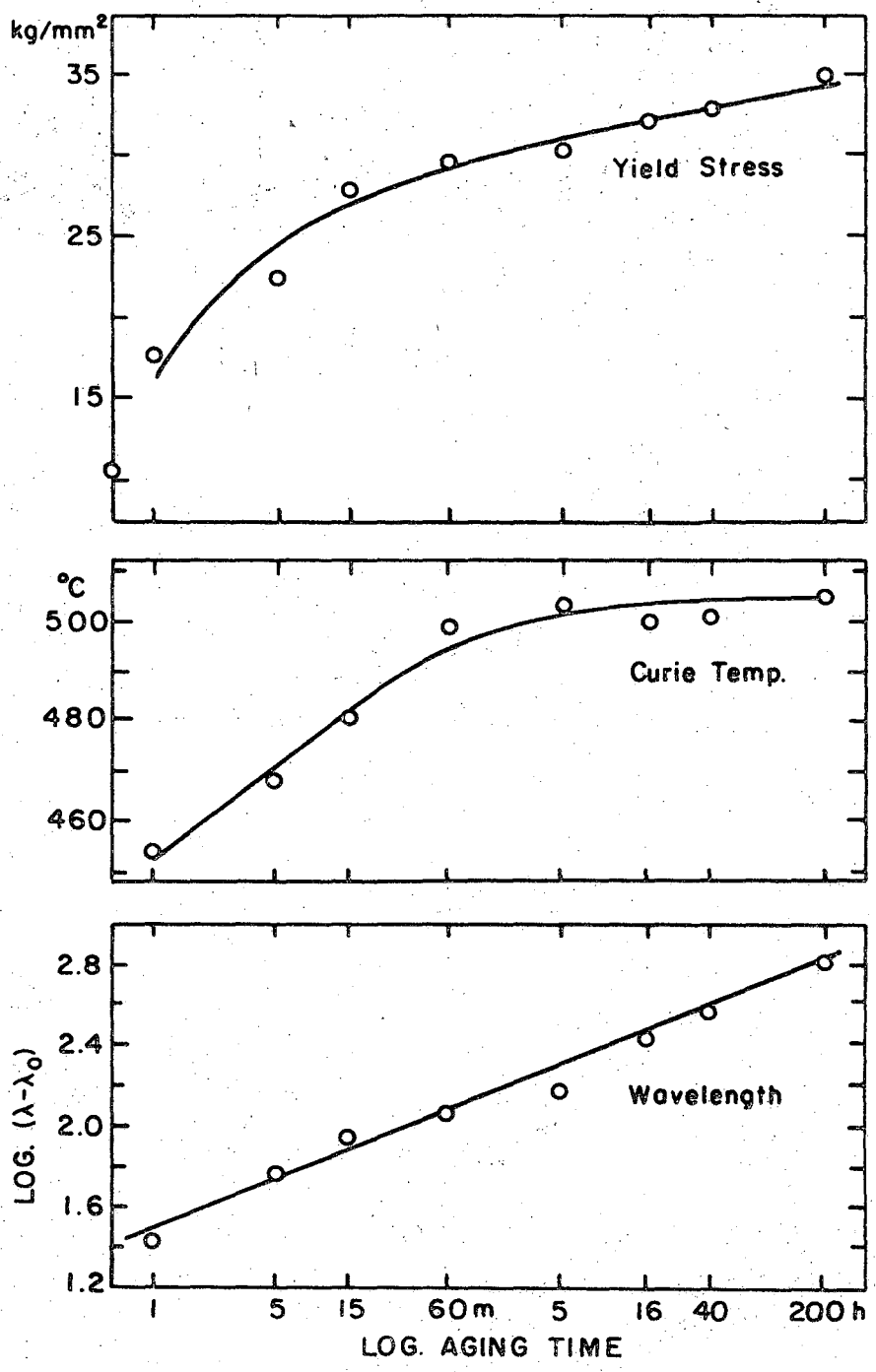

XBL 702-449

FIG. 5

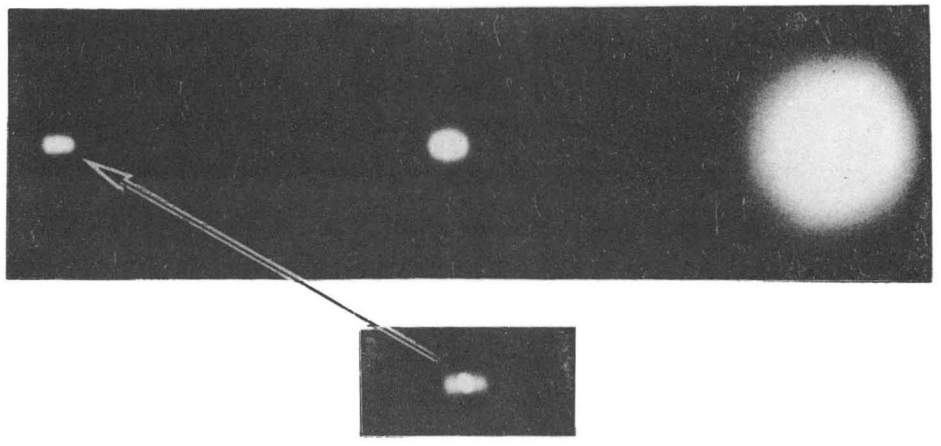

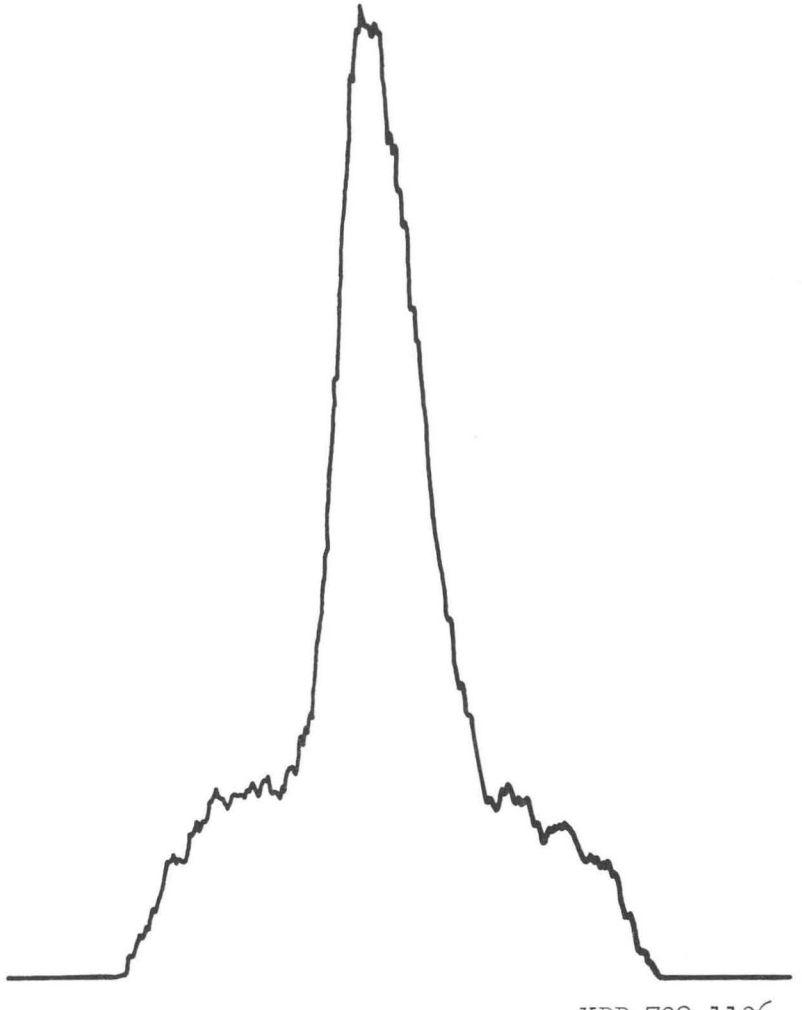

XBB 702-1106

Fig. 6

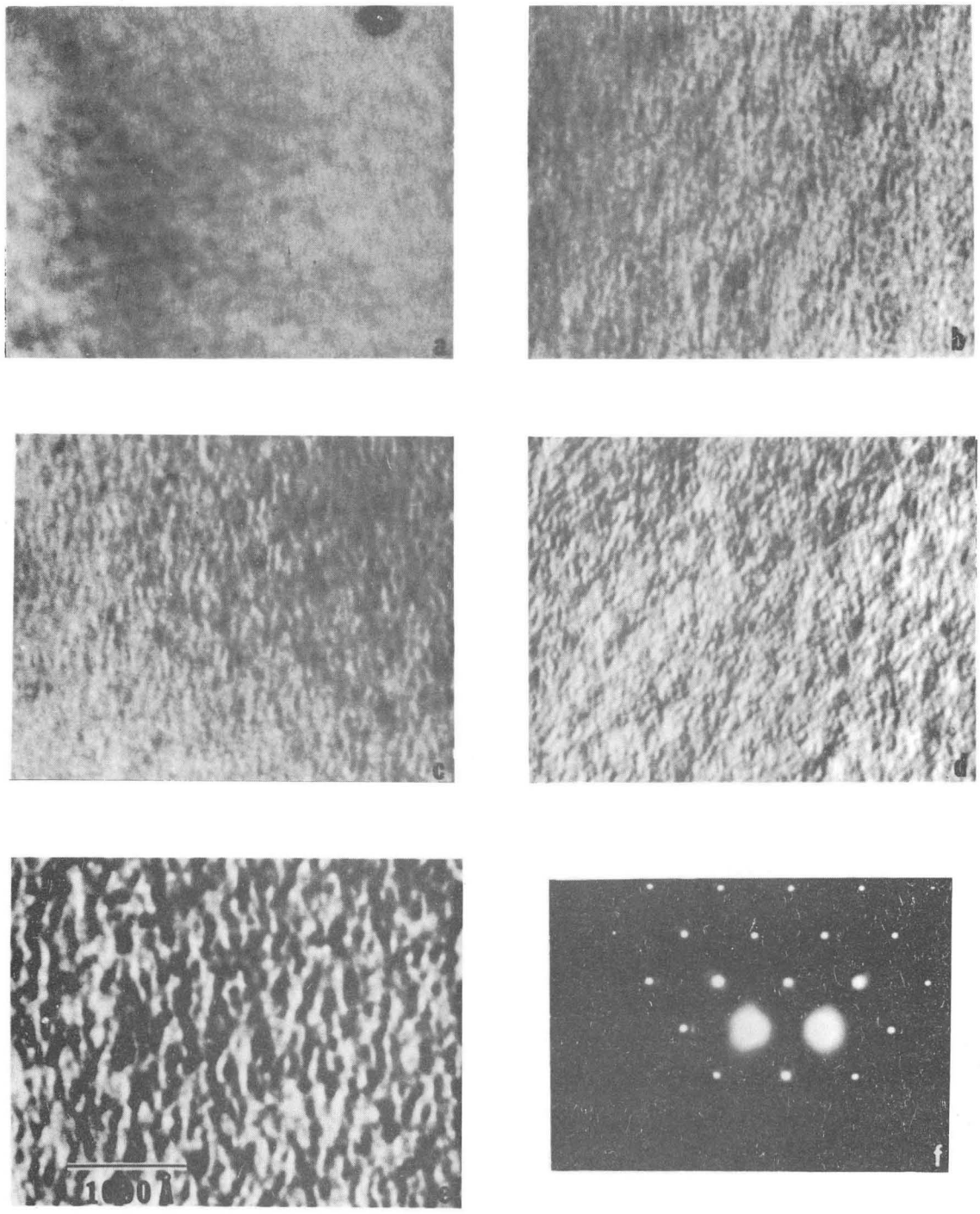

XBB 702-1105

Fig. 7

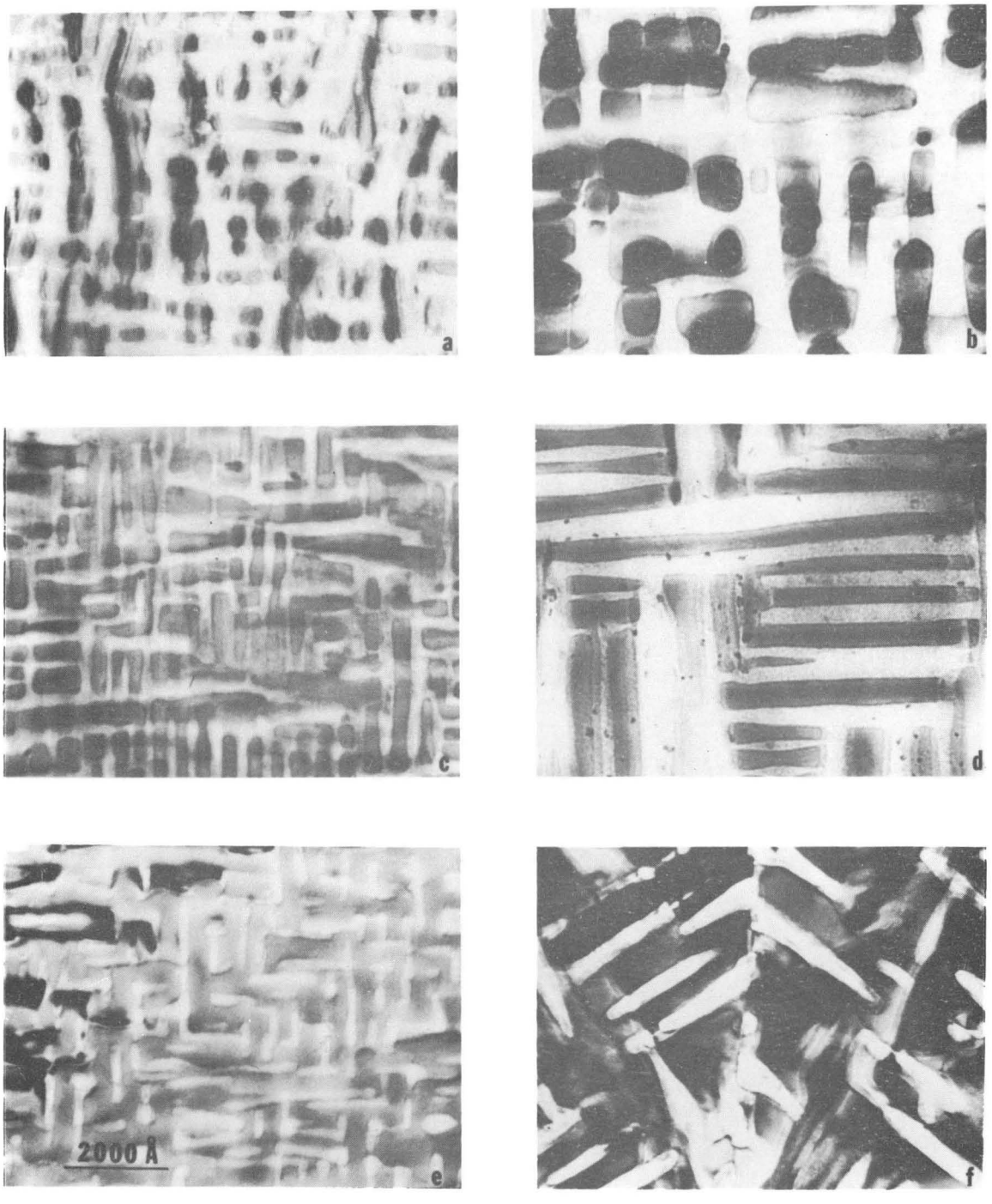

XBB 702-1104

Fig. 8

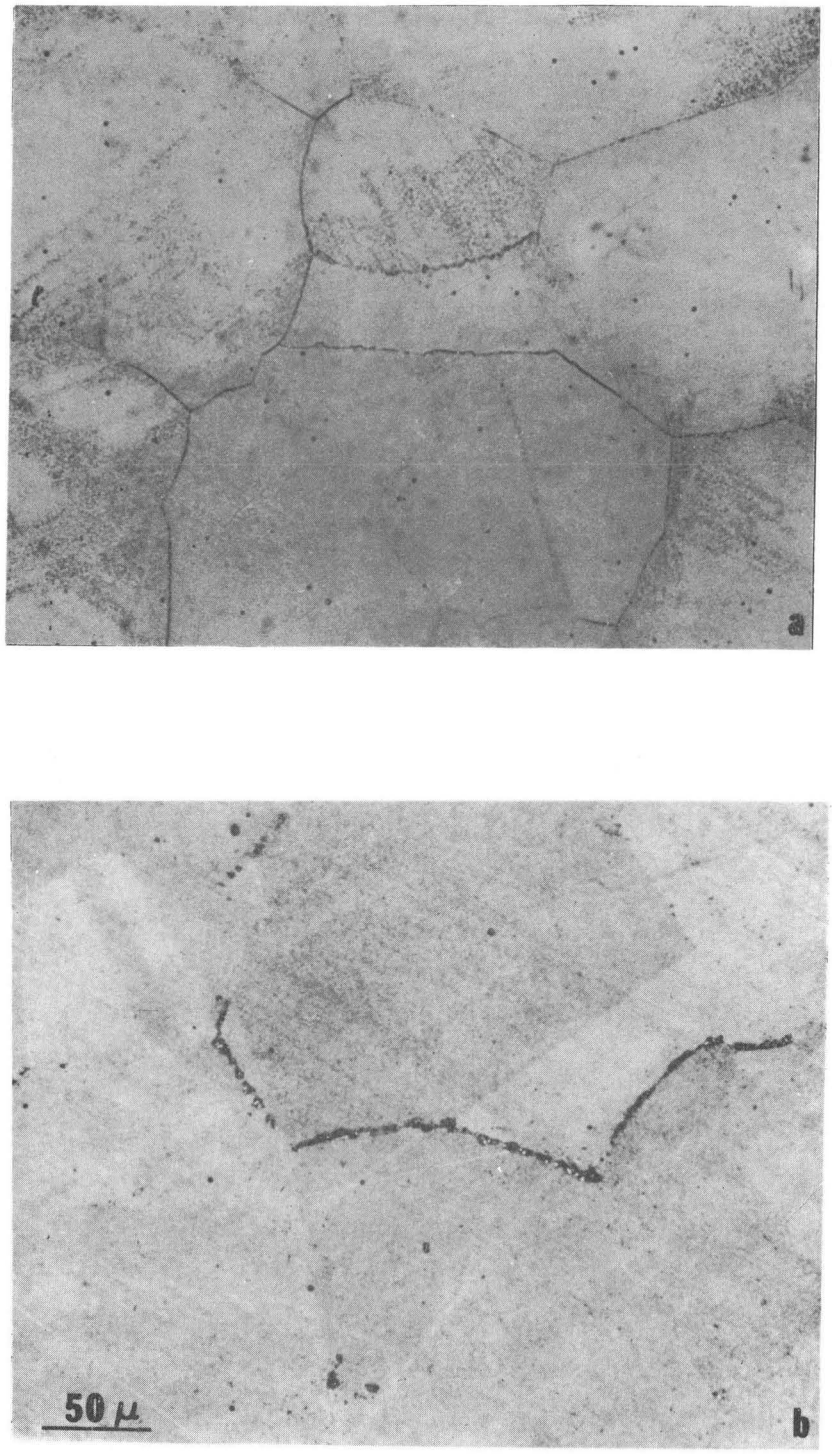

XBB 702-1102

Fig. 9

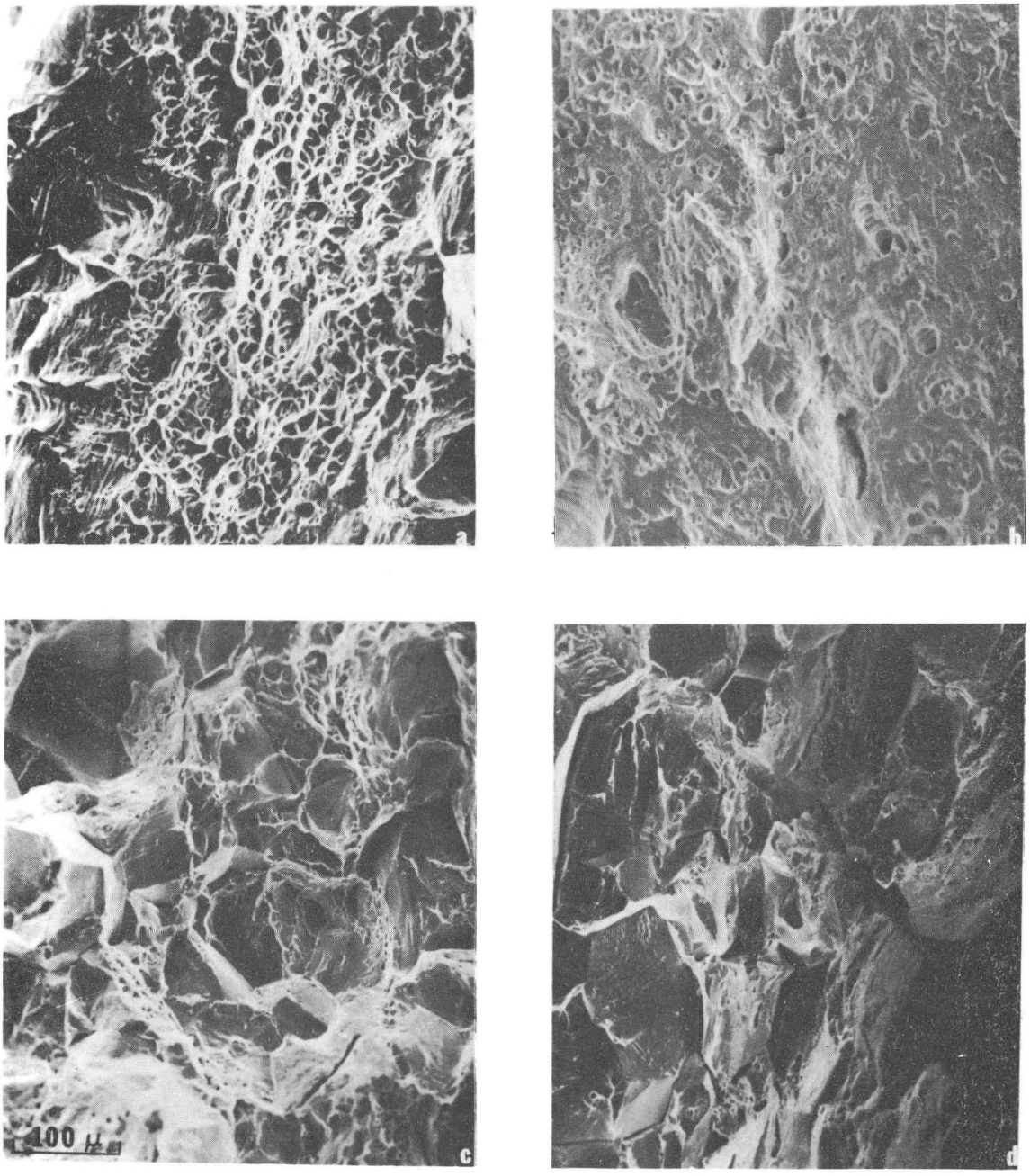

XBB 702-1103

Fig. 10

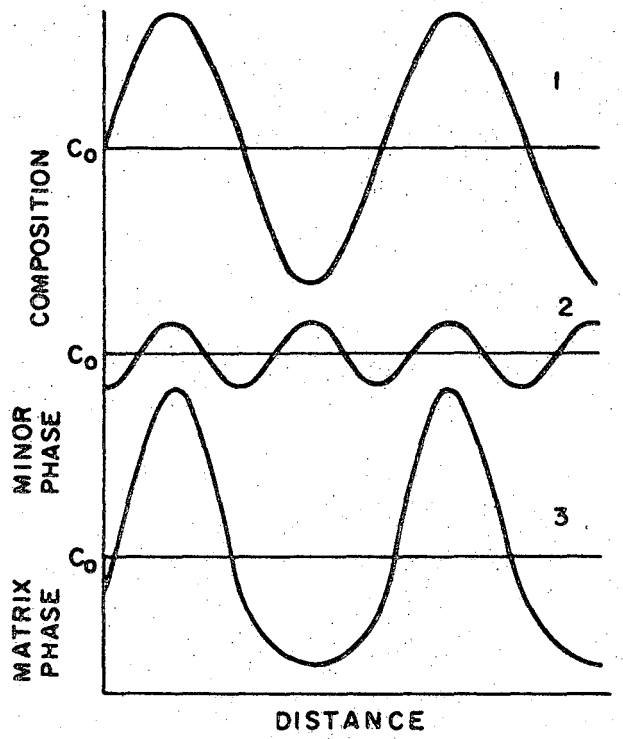

(a)

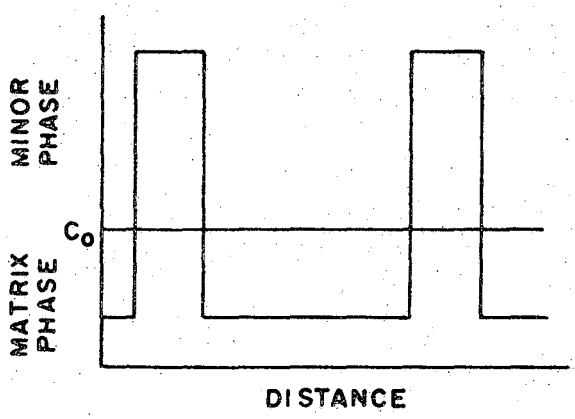

(b)

XBL 702-450

FIG. 11

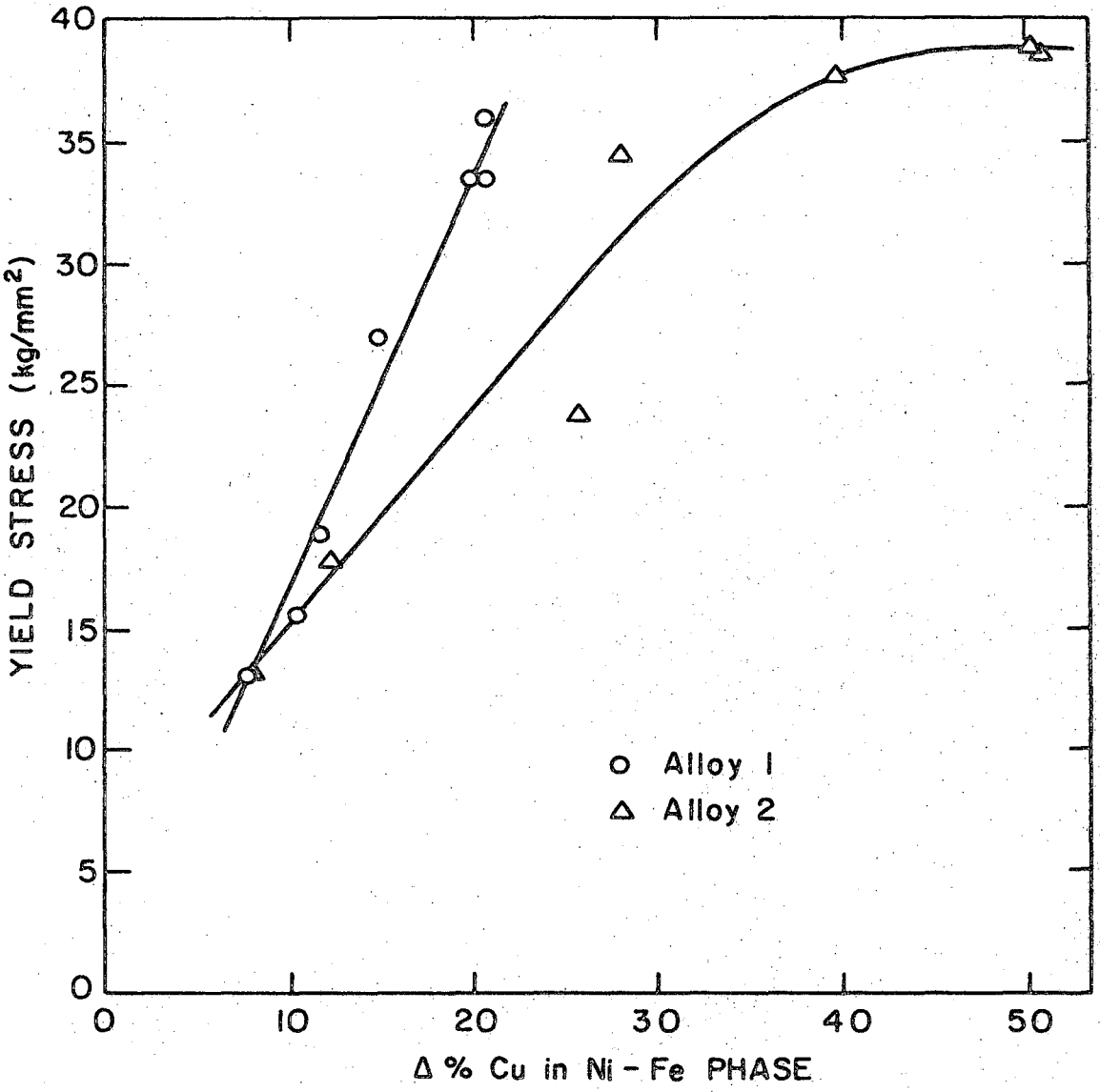

XBL 702-451

FIG. 12

TECHNICAL INFORMATION DIVISION
LAWRENCE RADIATION LABORATORY
UNIVERSITY OF CALIFORNIA
BERKELEY, CALIFORNIA 94720